*Journal of The Electrochemical Society*, **166** (12) D521-D529 (2019)
0013-4651/2019/166(12)/D521/9/$38.00 © The Electrochemical Society


# A Dynamic Mesh Method to Model Shape Change during Electrodeposition

**E. Karimi-Sibaki,[1] A. Kharicha,[1,z] M. Abdi,[1] M. Wu,[2] A. Ludwig,[2] and J. Bohacek[2]**

[1] *Christian-Doppler Laboratory for Metallurgical Applications of Magnetohydrodynamics, Montanuniversitaet of Leoben, A-8700 Leoben, Austria*
[2] *Chair of Simulation and Modeling of Metallurgical Processes, Montanuniversitaet of Leoben, A-8700 Leoben, Austria*

A novel dynamic mesh-based approach is proposed to simulate shape change of the deposit front during electrodeposition. Primary and secondary current distributions are computed. The proposed numerical model is tested on a two dimensional system for which analytical solutions was previously presented by Subramanian and White [J. Electrochem. Soc., 2002, C498-C505]. Firstly, calculations are carried out only in the electrolyte where the deposit front is considered to be the boundary of the computational domain. Secondly, a fully coupled simulation is carried out, and field structures such as electric potential and electric current density are computed both in the electrolyte and deposit. It is found that the deposit region must be included in calculations of primary current distribution as the magnitude of electric potential is inevitably non-zero at the deposit front during electrodeposition. However, the deposit front can be accurately tracked considering secondary current distribution with or without involving the deposit region in our calculations. All transient results are shown through animations in the supplemental materials.
 [DOI: 10.1149/2.1241912jes]

Manuscript submitted May 10, 2019; revised manuscript received July 3, 2019. Published July 31, 2019.

Electrodeposition is an extensively used technique to produce metals, alloys, and composite materials. The main components of an electrodeposition cell are two metal electrodes and an electrolyte subjected to an electric power supply. The electrolyte is an ionic conductor where chemical species including the metal of interest are in the liquid state. The metal ions are reduced to metal atoms through the electrochemical reduction reaction. Whereby, the metallic ions in the electrolyte are converted to the deposited metal on a cathode surface.[1,2]

Electrodeposition is a multi-scale/multi-phase/multi-physics process that involves several phenomena and their interactions. Heat transfer, chemical and electrochemical reactions, electric current density, ionic concentrations, and interactions between flow and magnetic field as known as magnetohydrodynamics (MHD) play decisive roles in the process. The thickness and shape (profile) of the deposited materials are indicators which are often used to determine the performance of the process. Therefore, it is of great importance to develop transient models which enables us to track the deposit-electrolyte interface and to compute transport phenomena in the electrolyte.

An extensive review of the computation of current distribution including primary and secondary during electrodeposition was given by Dukovic.[3] The primary current distribution ignores influences of concentration of ions in the electrolyte and electrode kinetics on the distribution of electric current density in the electrochemical cell. Therefore, the electrical resistance in the electrolyte is assumed to obey Ohm's law. Similarly, the secondary current distribution ignores composition variations in the electrolyte. Accordingly, Ohm's law is applied to solve Laplace equation, in which an effective electrical conductivity for the uniform electrolyte solution is considered. However, the potential drop at the electrode-electrolyte interface as a consequence of Faradaic reactions (electrode kinetics) is taken into account through Butler-Vomer formula.[4]

Customarily, Finite Element Method (FEM)[5–7] or Finite Difference Method (FDM) was applied to discretize the governing equations.[8–13] The numerical algorithm must include a procedure to track the deposition front. For that purpose, Monte Carlo technique,[12] Phase-Field modeling,[13] Boundary Element Method (BEM),[7] and Level-Set method[8–11] were previously utilized. The governing partial differential equations (PDE) demand the thermodynamic statement of free energy or entropy using Monte Carlo or Phase-Field modeling. The PDE are reformulated as integral equations in BEM method that in turn exerts a significant restriction on the range and generality of non-linear problems to which the method can effectively be applied.[14]

Generally, simulation of electrodeposition for large scale processes requires computation of the flow field. The Level-Set method is the most suitable procedure amongst the aforementioned techniques. Level-Set[9] as well as Volume of Fluid (VOF)[15,16] are adequate methods to calculate the interactions of field structures such as electric, heat, and flow fields in the presence of an interface between two materials. However, special care must be taken to model the electric current density at the interface. A diffuse interface is considered as a smooth transition layer with electrical conductivity between the conductivities of the electrolyte and deposit. This region covers several computational cells spanning the exact location of the interface. The complexity of the method arises once a specific condition (e.g. Butler-Volmer kinetics for secondary current distribution) must be applied at the deposit-electrolyte interface.[9]

Here, we propose a novel approach using the dynamic mesh technique for transient simulation of electrodeposition. The Finite Volume Method (FVM) is applied to discretize governing equations. FVM automatically satisfies the conservation of the desired variables such as mass, heat, concentration of ions and electric current density.[17] Previously, we successfully applied the dynamic mesh approach to study shape change during the melting of an ESR electrode considering interactions between flow, thermal, and electromagnetic fields.[18] Indeed, the proposed dynamic mesh based model enables us to construct a sharp deposit-electrolyte interface that is thoroughly accessible to assign any sort of boundary conditions for the fields of interest e.g. flow, concentration of ions, electric current density, etc. Furthermore, computations of transport phenomena can be carried out both in the electrolyte and deposit.

In this study, the proposed model is examined on a two dimensional system for which analytical solutions was previously presented by Subramanian and White.[19] Both primary and secondary current distributions are evaluated. Following Subramanian and White,[19] only the electric potential field is solved. Firstly, the computations are carried out in the electrolyte where the moving deposit-electrolyte is considered as the boundary of the computational domain. Secondly, we calculate field structures in both electrolyte and deposit in which the moving interface is modeled as a conjugate wall that fully couples two separated regions. The latter helps us to scrutinize the necessity of involving the deposit region in the modeling of electrodeposition processes.

## Modeling

Subramanian and White[19] developed a semi-analytical method considering both primary and secondary current distributions to simulate shape change during electrodeposition. They investigated a 2D electrochemical cell that is shown in Fig. 1. Their study is considered as the benchmark to assess our modeling approach. As shown in Fig. 1,

[z] E-mail: Abdellah.kharicha@unileoben.ac.at

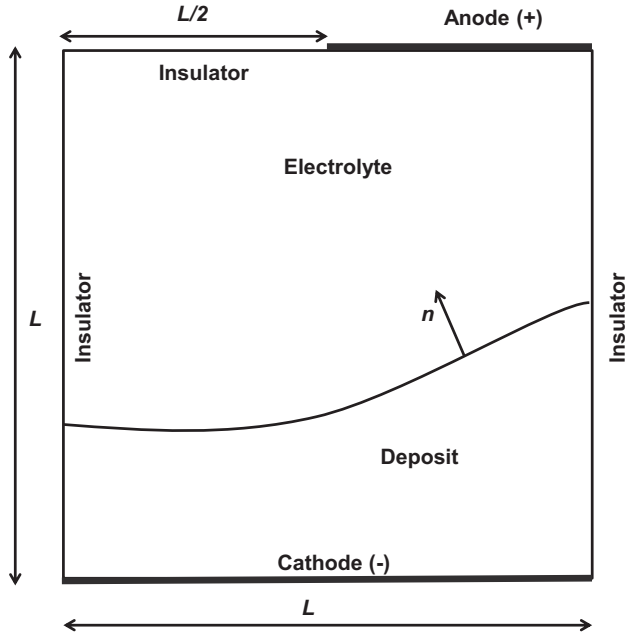


**Figure 1.** Configuration of the computational domain and boundaries are illustrated. *n* is the normal vector to the deposit front.

the cathode (−) is located at the bottom of the cell, whereas the anode (+) is coplanar with the upper insulating plane. The side walls are electrically insulated. The system operates under a constant applied voltage where the composition of the electrolytic solution is assumed to remain uniform. The electrodeposition occurs at the cathode surface.

The speed of growing deposit ($u_d$) is governed by the magnitude of current density ($j$) normal to the deposit-electrolyte interface as follows:

$$u_d = -\frac{M}{zF\rho} j \quad [1]$$

Where $M$ is the molecular weight, $z$ is number of exchanged electrons, $F$ is Faraday constant, and $\rho$ is the density of the deposited material. Of note, the correlation $\frac{M}{zF\rho}$ in Eq. 1, is generally a constant value which is dependent on material properties. The constant has no influence on the shape (profile) of the growing deposit. However, the constant can influence the required time to deposit a certain amount of material.

***Electric current density field.—***The conservation equation of electric current density is given by,

$$\nabla \cdot (-\kappa \nabla \varphi) = 0 \quad [2]$$

The electric current density is linearly dependent on the electric field ($E = -\nabla\varphi$) that in turn is governed by the gradient of the electric potential ($\varphi$),

$$j = \kappa \vec{E} \quad [3]$$

In Eqs. 2 and 3, the correlation is referred as the electrical conductivity ($\kappa$).

The value of electric potential is fixed at the anode. The flux of electric potential ($\approx$ electric current density) is set to zero at insulating walls. Here, the cathode is of prime interest where electrodeposition takes place. The major difference between the primary and secondary current distribution is the treatment of boundary condition for electric potential at the growing deposit boundary (cathode). The value of electric potential is set to zero at the cathode in primary current calculation. However, the current density ($\approx$ flux of electric potential) obeys Butler-Volmer kinetics at the cathode surface for secondary current distribution as follows:

$$j = j_0 \left[ e^{\alpha z F \varphi / RT} - e^{-(1-\alpha) z F \varphi / RT} \right] \quad [4]$$

Where $j_0$ is exchange current density, $R$ is universal gas constant, $T$ is temperature, and $\alpha$ denotes charge transfer coefficient.

**Table I. Parameters used in our calculations. Dimensionless form of the equations regarding to primary and secondary current distributions are solved. Considering the dimensionless parameters, the system well represents the cathodic deposition of copper in copper sulfate solution at room temperature.**

| Parameter | |
|---|---|
| $R\ [J\ K^{-1} mol^{-1}]$ | 8.314546 |
| $T\ [K]$ | 293 |
| $F\ [A\ s\ mol^{-1}]$ | 96485 |
| $k\ [S\ m^{-1}]$ | 5.1 |
| $j_0\ [A\ m^{-2}]$ | 5 |
| $L\ [m]$ | 0.01 |
| $z$ | 2 |
| $\alpha$ | 0.5 |
| $I_0$ | 1 |
| $\varphi_A^*$ | 1 |
| $\nu$ | 0.48 |

Subramanian and White[19] reformulated the given standard equations to dimensionless forms. The dimensionless variables are as follows:

$$\varphi^* = \frac{zF\varphi}{RT} \quad [5]$$

$$\frac{\partial \varphi^*}{\partial n} = -I_0 \left[ e^{\alpha \varphi^*} - e^{-(1-\alpha)\varphi^*} \right] \quad [6]$$

Where, $n$ is the vector normal to the growing deposit surface, $\varphi^*$ denotes the dimensionless electric potential, $I_0 = \frac{j_0 zLF}{\kappa RT}$, and $L$ is the characteristic length of the system.

For further information regarding to the derivation of the dimensionless form of the governing equations, the interested readers are highly encouraged to consult Ref. 19.

***Dynamic mesh.—***Dynamic mesh is a powerful technique to model deformable boundaries in which the mesh nodes are re-adjusted to new locations. One should keep in mind that all modeling equations presented in this section have no influence on the growing deposited velocity or any other transport parameter such as electric potential. They only serve to update the mesh inside the continuously deforming computational domain.

The general transport equation including advection and diffusion for $\zeta$ as an arbitrary variable (e.g. heat, concentration of ion, etc.) is expressed as:

$$\frac{\partial \rho \zeta}{\partial t} + \nabla \cdot (\rho u \zeta) = \nabla \cdot (\Gamma \nabla \zeta) + S_\zeta \quad [7]$$

Where $u$ denotes velocity, $\Gamma$ is the diffusion coefficient, $t$ is time, and $S_\zeta$ is the volumetric source term. In order to utilize this technique, all governing transport equations must take into account the velocity of the grid boundary ($u_g$).[20] Correspondingly, the integral form of Eq. 7 with respect to dynamic mesh is given by:

$$\frac{\partial}{\partial t} \int_V \rho \zeta dV + \int_\Omega \rho \zeta \left( \vec{u} - \vec{u_g} \right) \cdot d\vec{S} = \int_\Omega \Gamma \nabla \zeta \cdot d\vec{S} + \int_V S_\zeta \, dV \quad [8]$$

Where $\Omega$ represents the boundary of the control ($V$), and $\vec{S}$ denotes the area vector. In Eq. 8, the unsteady term accounts for the variation in the size of each computational cell during the calculation, and subsequently that is computed using the grid velocity[21] as follows:

$$\frac{\partial V}{\partial t} = \sum_i^{n_f} \vec{u_i} \cdot \vec{S_i} \quad [9]$$

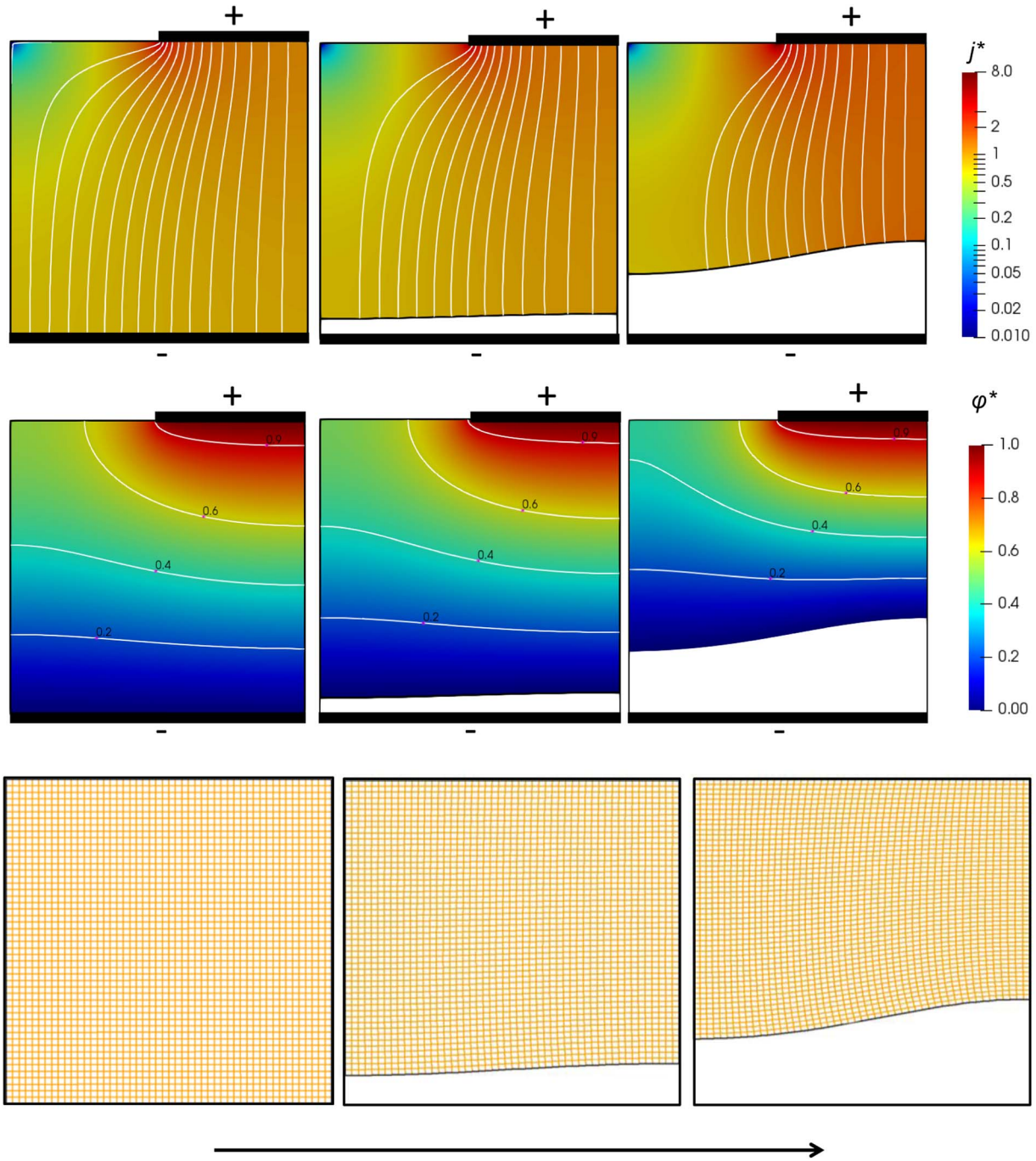


**Figure 2.** Considering primary current distribution, snapshots at different times of field structures are shown: (First row) The magnitude and streamlines of the dimensionless electric current density ($j^* = j/j_0$); (Second row) Contour of dimensionless electric potential and isolines of the dimensionless electric potential including 0.2, 0.4, 0.6, and 0.9 are shown. (Third row) For illustrative purposes, the deformation of the coarse mesh is shown. The arrow indicates time-advancement.

Where $n_f$ is the number of faces which belongs to the control volume, $\vec{u}_i$ and $\vec{S}_i$ are the velocity and area vector of $i$ face respectively.

Herein, the smoothing scheme is applied to handle the boundary motion.[20] Accordingly, the interior nodes of the computational domain are repositioned as the boundary (growing deposit) moves. They can be re-located but the connectivity between them must remain unchanged. During the transient calculations, the interior nodes conform to a network of interconnected springs, and consequently, their positions are updated at each time step based on displacements of boundary nodes. The displacements of the interior nodes ( $\vec{y} = \int \vec{u}_i dt$ ) are determined according to the linearly elastic solid model.[20] The following set of equations govern the mesh motion,

$$\nabla \cdot \sigma\ (\vec{y}) = 0 \qquad [10]$$

$$\sigma\ (\vec{y}) = \lambda\,(tr\varepsilon\,(\vec{y}))\,I + 2\mu\varepsilon\,(\vec{y}) \qquad [11]$$

$$\varepsilon\ (\vec{y}) = \frac{1}{2}\left(\nabla\vec{y} + (\nabla\vec{y})^T\right) \qquad [12]$$

Where $\sigma$ is the stress tensor that is composed of strain tensor ($\varepsilon$), the trace of strain tensor ($tr\varepsilon$), identity matrix ($I$), shear modulus ($\mu$), and Lame's first parameter ($\lambda$). Specifying the ratio ($\mu/\lambda$) is sufficient to solve the whole set of Eqs. 10–12 that is defined through Poisson's

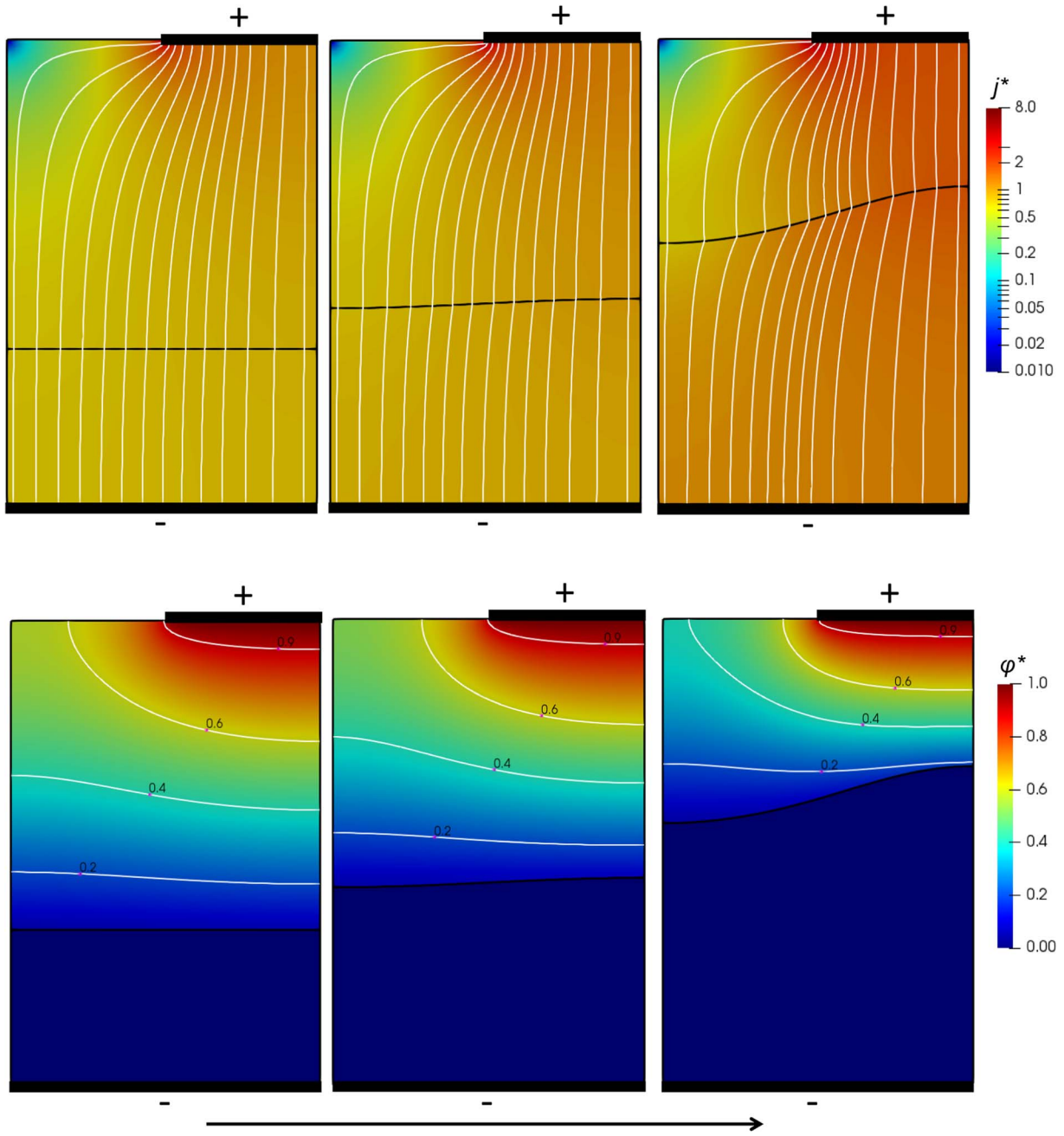


**Figure 3.** Considering primary current distribution for coupled simulation, snapshots at different times of field structures are shown: (First row) The magnitude and streamlines of the dimensionless electric current density ($j^* = j/j_0$); (Second row) Contour of dimensionless electric potential and isolines of the dimensionless electric potential including 0.2, 0.4, 0.6, and 0.9 are shown. The arrow indicates time-advancement.

ratio ($\nu$),[20]

$$\nu = \frac{1}{2\left(1 + \frac{\mu}{\lambda}\right)} \qquad [13]$$

The ratio is a user-input parameter. To preserve the orthogonal quality of the mesh, we recommend assigning the value of $\nu$ in the range between 0.45 and 0.5.

Boundary conditions for Eqs. 10–12 are straightforward. At the moving deposit-electrolyte interface the displacement is given that is calculated from Eq. 1. At the upper insulating plane and anode, the displacement is set to zero. Furthermore, the displacement normal to the boundary as well as stress tangential to the boundary is set to zero at insulating side-walls.

Once again, it must be emphasized that the linearly elastic solid model has no influence on the growing deposited velocity or any other transport parameter such as electric potential. The model solely serves to update the mesh by re-location of interior nodes at each time step in the perpetually deforming computational domain.

***Other settings.***—The commercial CFD software, ANSYS FLUENT v.17.1, was employed to carry out our simulations. The software comprises the dynamic mesh technique for the simulation of displacements of boundaries. User-defined functions (UDF) are implemented for special modeling equations such as Butler-Volmer formula, speed of growing deposit, etc. The model is configured based on the study which was conducted by Subramanian and White.[19] Accordingly, governing equations are solved in the dimensionless form.

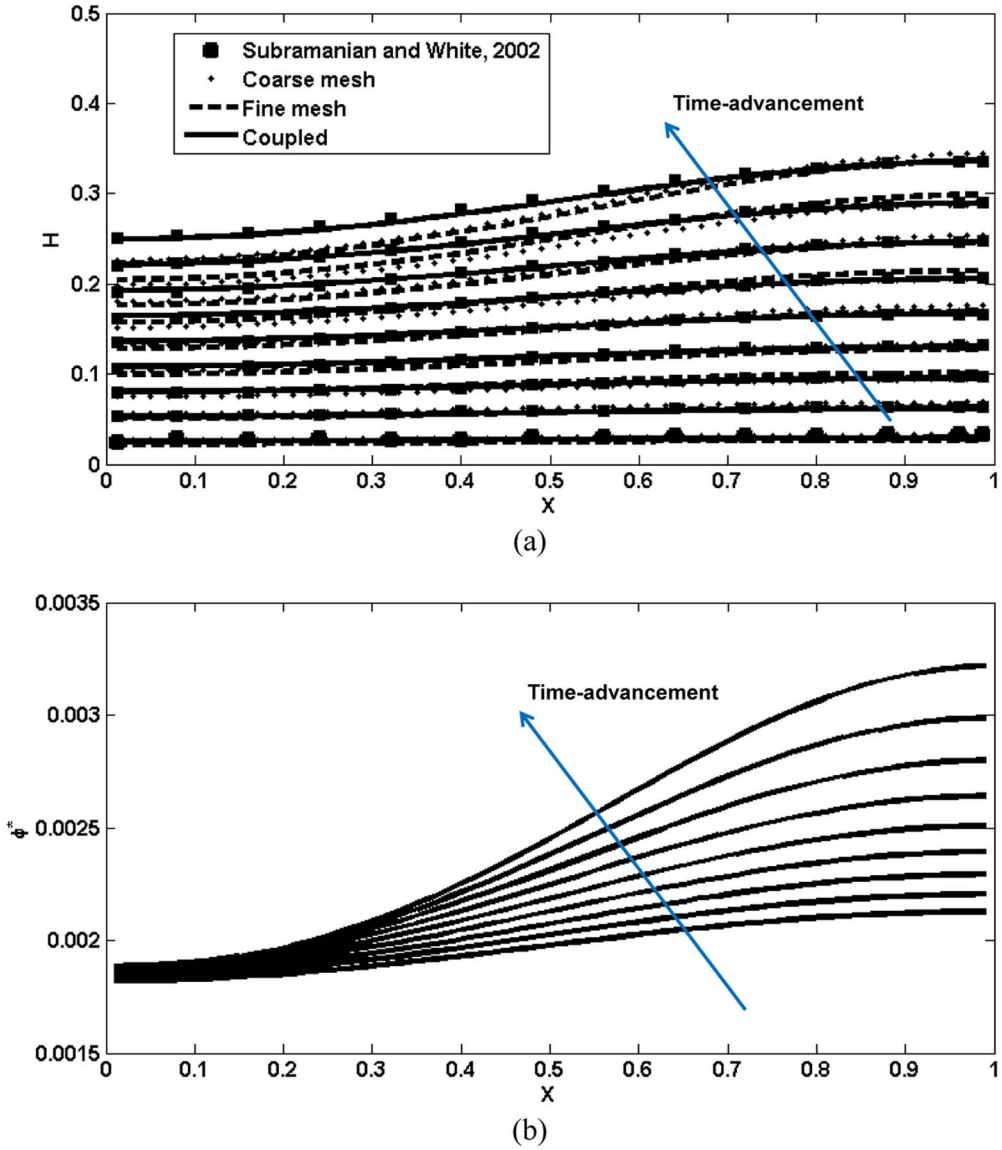


**Figure 4.** Considering primary current distribution, (a) the dimensionless deposit thickness ($H = h/L$) is plotted versus the dimensionless distance along the cathode ($X = x/L$) to illustrate the transient shape change during electrodeposition; (b) dimensionless electric potential on the deposit front is plotted versus the dimensionless distance along the cathode ($X = x/L$).

The geometry is illustrated in Fig. 1. The computational domain initially contains structured equisized elements. To explore the influence of grid size on the outcome, two different sizes of mesh element are examined namely coarse mesh and fine mesh. The characteristic size of the domain is: L = 1 cm. The coarse mesh computational domain is filled by 2500 elements with the size of 0.2 mm. The fine mesh contains 10000 elements with the element size of 0.1 mm. Furthermore, another investigation namely coupled is carried out to calculate field structures in both electrolyte and deposit. For the latter, it is assumed that the initial deposit height is L/2 whereas the initial electrolyte height is kept to L. In addition, it is assumed that the electrical conductivity of deposit is five orders of magnitude ($10^5$) higher than that of electrolyte. Parameters used in our calculations are listed in Table I. The electric potential at the anode ($\boldsymbol{\varphi}_A^* = 1$) is fixed in all of our calculations.

## Results and Discussion

Transient calculations are performed and the deposit front, deformation of the grid in the computational domain, and field structures such as electric current density and electric potential were captured. It is not possible to effectively demonstrate those parameters using images although some snapshots of different times are shown in this section. We highly encourage readers to observe supplemental materials related to the present paper. For all case studies, the aforementioned parameters are shown through animations.

***Primary current distribution.—***The electric current density flows from anode (+) toward the cathode (−) which is the deposit front where the electric potential is set to zero. Demonstratively, snapshots at different times of the magnitude of the electric current density and the trajectory of the electric current are shown in Fig. 2. The maximum amount of electric current density is near the edge of anode. As deposit thickness increases, the amount of electric current density which flows through the electrolyte increase especially near the upper edge of deposit front. At constant applied voltage, with the increase of deposit thickness the total electrical resistance of the system decreases. Consequently, a higher amount of electric current is allowed to flow through the system. Streamlines of electric current density are also shown to track the trajectory of electric current. The electric current

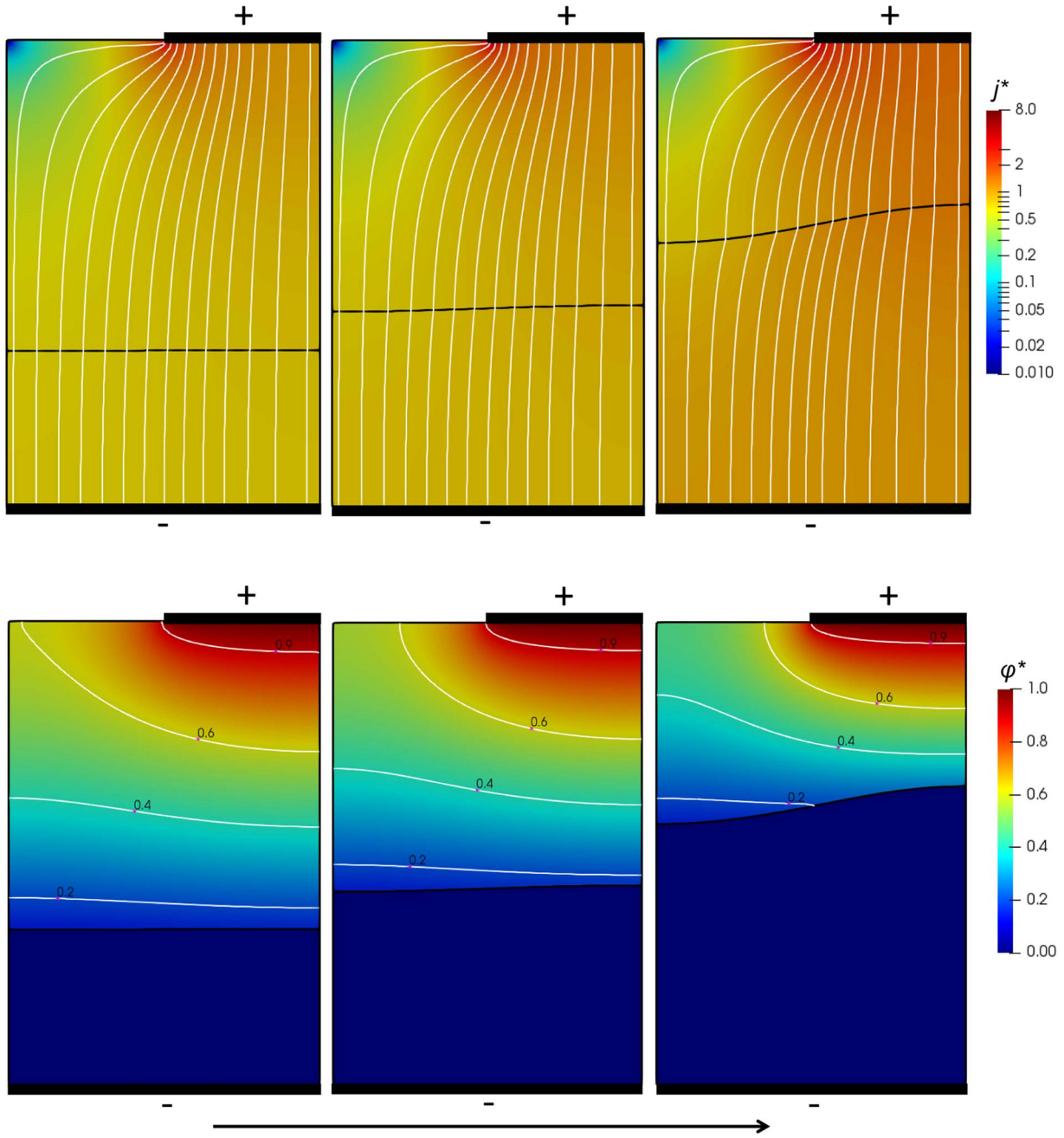


**Figure 5.** Considering secondary current distribution for coupled simulation, snapshots at different times of field structures are shown: (First row) The magnitude and streamlines of the dimensionless electric current density ($j^* = j/j_0$); (Second row) Contour of dimensionless electric potential and isolines of the dimensionless electric potential including 0.2, 0.4, 0.6, and 0.9 are shown. The arrow indicates time-advancement.

density is perpendicular to the surface of deposit front all along the surface. As illustrated in Fig. 2, the electric potential field continuously alters as the deposit front moves forward. The equipotential lines are always perpendicular to the stream lines of electric current density at each point inside the electrolyte. For illustrative purposes, snapshots at different times of the evolving coarse grid are shown in Fig. 2. The deformation of deposit front is imitated by the nearby mesh that in turn enables us to achieve high orthogonality of mesh elements, and consequently, to preserve the quality of mesh. All transient results are provided in supplemental materials. Readers are encouraged to observe "Primary-Coarse-Mesh.avi" and "Primary-Fine-Mesh.avi" files.

Fig. 3 illustrates modeling results of a coupled simulation for which calculations of field structures are carried out both in the electrolyte and deposit. The electric potential is set zero at the cathode. Additionally, the continuous transition of the electric potential is calculated at the deposit front during electrodeposition. As a consequence of ignoring the formation of electric double layer (EDL) in the calculation of primary current distribution, no electrical resistance exists at the deposit front. In the modeling point of view, the deposit front is treated as a conjugate wall where the electric potential on both sides (electrolyte side and deposit side) are equal to each other. Snapshots at different times of electric current density and electric potential fields are shown in Fig. 3. Similar to the previous calculation, the current density is perpendicular to the surface of deposit front. However, streamlines of electric current bend just at the moment they enter to the non-flat deposit front. As shown in Fig. 3, the electric field (gradient of electric potential) remains very weak in the deposit region during the

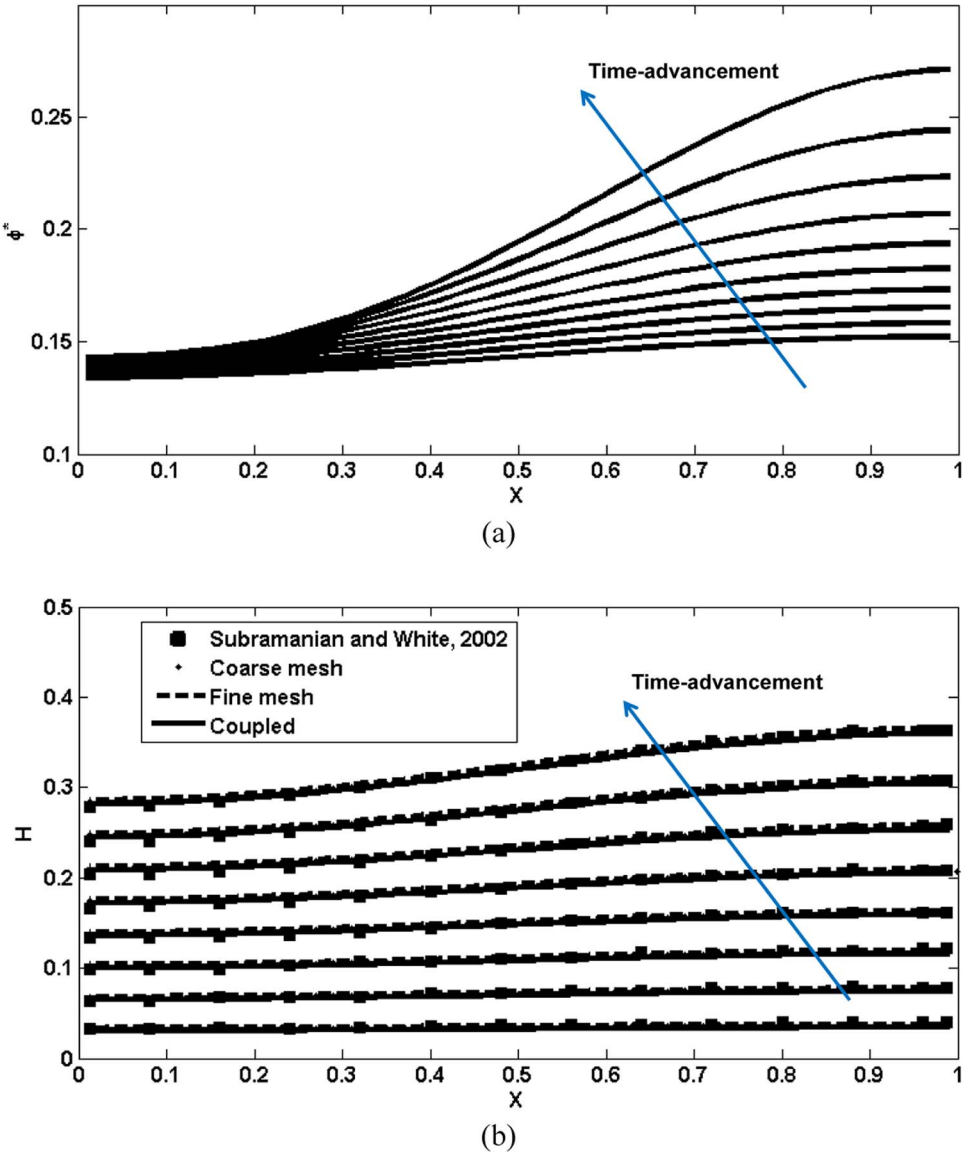


**Figure 6.** Considering secondary current distribution, (a) dimensionless electric potential on the deposit front is plotted versus the dimensionless distance along the cathode ($X = x/L$); (b) the dimensionless deposit thickness ($H = h/L$) is plotted versus the dimensionless distance along the cathode ($X = x/L$) to illustrate the transient shape change during electrodeposition.

process. All transient results of this system are provided in supplemental materials as "Primary-Coupled.avi".

A comparison is made between the calculated deposition thickness using our model and that of Subramanian and White[19] as shown in Fig. 4a. Computed results using fine or course meshes are relatively similar. Ignoring the deposit region in our calculations, the discrepancy between our modeling results and analytical results increase as the thickness of deposition increases. Principally, assuming zero value for the electric potential at the deposit front is erroneous although this assumption may greatly simplify the problem. It was pointed out that the error in this approximation drastically increases as the electric current density increases.[9] A good agreement between our modeling results and analytical results is obtained for the coupled simulation. As shown in Fig. 4b, the electric potential at deposit front is minimal but non-zero. Furthermore, the magnitude of electric potential continuously changes along the deposit front during the electrodeposition process. In fact, the magnitude of electric potential is always non-zero at the deposit front as the existence of an electric field (gradient of electric potential) is essential to flow electric current through the deposit region.

***Secondary current distribution.***—Here, results regarding to the secondary current distribution are presented in a similar manner to results of primary current distribution. Calculations considering coarse mesh, fine mesh, and coupled were carried out. We suggest observing "Secondary-Coarse-Mesh.avi" and "Secondary-Fine-Mesh.avi" files which are provided in supplemental materials where variations in field structures in the electrolyte during electrodeposition are demonstrated. Snapshots at different times of electric current density and electric potential fields in both electrolyte and deposit are shown in Fig. 5. Those are obtained through the coupled simulation. From a modeling point of view, the deposit front is a conjugate wall where the influence of the formation of EDL (more precisely Butler-Volmer kinetics) is implicitly modeled. The fluxes of electric potential ($\approx$ electric current density) on both sides of the conjugate wall (electrolyte side and deposit side) are equal to each other, whereas the electric potential magnitudes are unequal. Streamlines of electric current density indicate the trajectory of the electric current density. They are perpendicular to equipotential lines at each point inside the electrolyte. At the very deposit-electrolyte interface, the electric current density is perpendicular to the surface of deposit front where the flux of electric potential is specified. On

the other hand, a noteworthy amount of electric current density flows tangential to the deposit front adjacent to deposit-electrolyte interface in the electrolyte region. Therefore, the electrical streamlines do not appear completely perpendicular to the deposit front in Fig. 5. The variation in electric potential at deposit front during the process is plotted in Fig. 6a. A notable difference in electric potential is recognized along the surface of deposit front where electric current can flow in tangential direction to the deposit front in the electrolyte region (more precisely outside of the EDL in the bulk of electrolyte). As shown in Fig. 6b, computed thickness of deposition layer is compared with analytical results.[19] A good agreement is observed between our modeling results including coarse mesh, fine mesh, and coupled with analytical results. This implies that, it is not necessary to include calculations of field structures in the deposit region considering secondary current distribution to capture transient thickness of deposition layer. All transient results regarding to secondary current distributions are available in supplemental materials including "Secondary-Coarse-Mesh.avi", "Secondary-Fine-Mesh.avi", and "Secondary-Coupled.avi".

It is well-known that a higher uniformity for the thickness of deposit along the cathode can be achieved for secondary current distribution than that of primary current distribution.[2,3] This implies that the electric current density is more evenly distributed along the deposit front for secondary current distribution compared to that of primary current distribution. The variation in the magnitude of electric current density at deposit front during the process is plotted in Fig. 7 considering primary and secondary current distributions. The total electrical resistance of the system decreases as deposit thickness increases. Consequently, the amount of electric current density which flows through the system increases as time advances. The secondary current distribution as shown in Fig. 7b exhibits a higher uniformity of the distribution of electric current density along the cathode compared to that of primary current distribution which is shown in Fig. 7a.

Over the past decade, authors of the present study developed numerous models to study transport of ions by advection, diffusion, and electro-migration.[22–25] In addition, the dynamic mesh tool was successfully used to study shape change during the melting of an ESR electrode considering interactions between flow, thermal, and electromagnetic fields.[18] We believe that the proposed dynamic mesh model has a promising future to accurately handle the aforementioned transport phenomena. In the near future, we plan to include those

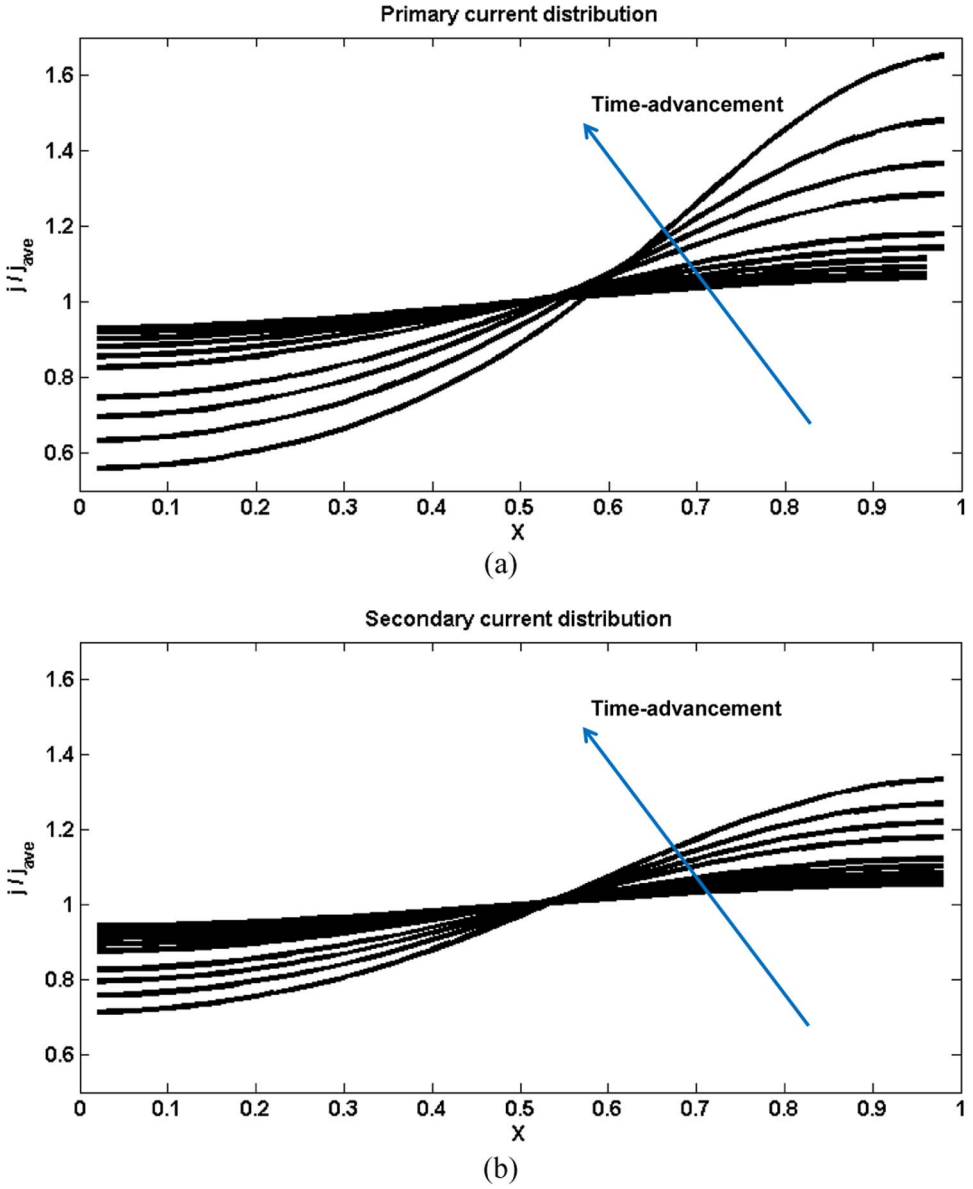


**Figure 7.** Normalized electric current density on the deposit front is plotted versus the dimensionless distance along the cathode ($X = x/L$). $j_{ave}$ denotes the average current density that flows across the deposit front. The arrow indicates time-advancement. (a) Primary current distribution; (b) Secondary current distribution.

modeling features to investigate electrodeposition during actual industrial processes.[13,26,27]

## Summary

We propose a novel approach using dynamic mesh technique to model shape change during electrodeposition. The model is tested on a two dimensional system for which analytical solutions is available. Primary and secondary current distributions are computed. The proposed transient model enables us to track the deposit front while field structures such as electric potential and electric current density fields are continuously evolving. This numerical approach requires updating of the mesh on each time step. For that purpose, a linearly elastic solid model is employed to continuously relocate interior nodes within the computational domain. Firstly, calculations are carried out only in the electrolyte considering different mesh sizes where the deposit front is the boundary of the computational domain. Secondly, a fully coupled simulation is carried out to compute field structures both in the electrolyte and deposit. It is found that incorporating the deposit region (coupled simulation) considering primary current distribution is necessary to correctly capture the deposit thickness as the magnitude of electric potential is unavoidably non-zero at the deposit front. However, the deposit front is accurately tracked considering secondary current distribution with or without involving the deposit region in our calculations. Although the current study is purely a fundamental research, we believe that the proposed approach has a promising future to simulate actual industrial processes involving electrodeposition phenomenon. All transient results are shown through animations in supplemental materials. Therefore, we highly recommend readers to observe supplemental materials related to the present paper.

## Acknowledgments

The authors acknowledge financial support from the Austrian Federal Ministry of Economy, Family and Youth and the National Foundation for Research, Technology and Development within the framework of the Christian-Doppler Laboratory for Metallurgical Applications of Magnetohydrodynamics.

## ORCID

E. Karimi-Sibaki https://orcid.org/0000-0002-2275-6699

## References

1. M. Paunovic and M. Schlesinger, Fundamentals of Electrochemical Deposition. Wiley, New York, 1998.
2. Y. D. Gamburg and G. Zangari, Theory and Practice of Metal Electrodeposition, Springer-Verlag, New York, 2011.
3. J. O. Dukovic, Computation of current distribution in electrodeposition, a review, *IBM Journal of Research and Development*, **34**(5), 693 (1990).
4. J. Newman and K. E. Thomas-Alyea, Electrochemical Systems. John Wiley & Sons, New Jersey, 2004.
5. R. Alkire, T. Bergh, and R. L. Sani, Predicting Electrode Shape Change with Use of Finite Element Methods, *J. Electrochem. Soc.*, **125**(12) (1978).
6. A. Mahapatro and Kumar Suggu S, Modeling and simulation of electrodeposition: Effect of electrolyte current density and conductivity on electroplating thickness, *Adv. Mater. Sci.*, **3**(2), 1 (2018).
7. N. G. Zamani and F. H. Peters, Application of the boundary element method in electrodeposition problems, *Applied Mathematical Modelling*, **10**, 262 (1986).
8. D. Wheeler, D. Josell, and T. P. Moffat, Modeling Superconformal Electrodeposition Using the Level Set Method, *Journal of The Electrochemical Society*, **150**(5), C302 (2003).
9. M. Hughes, N. Strussevitch, C. Bailey, K. McManus, J. Kaufmann, D. Flynn, and M. P. Y. Desmulliez, Numerical algorithms for modelling electrodeposition: Tracking the deposition front under forced convection from megasonic agitation, *Int. J. Numer. Meth. Fluids*, **64**, 237 (2010).
10. D. Adalsteinsson and J. A. Sethian, A Level Set Approach to a Unified Model for Etching, Deposition, and Lithography, II: Three-dimensional Simulations, *Journal Computational Physics*, **122**, 348 (1995).
11. M. Georgiadou, D. Veyret, R. L. Sani, and R. C. Alkirea, Simulation of Shape Evolution during Electrodeposition of Copper in the Presence of Additive, *Journal of The Electrochem. Soc.*, **148**(1), C54 (2001).
12. T. O. Drews, S. Krishnan, J. C. Alameda, D. Gannon, R. D. Braatz, and R. C. Alkire, Multiscale simulations of copper electrodeposition onto a resistive substrate, *IBM Journal of Research and Development*, **49**, 49 (2005).
13. W. Pongsaksawada, A. C. Powell IV, and D. Dussault, Phase-Field Modeling of Transport-Limited Electrolysis in Solid and Liquid States, *J. Electrochem. Soc.*, **154**, F122 (2007).
14. M. Schanz, Wave Propagation in Viscoelastic and Poroelastic Continua, Springer, 2001.
15. A. Kharicha, M. Wu, and A. Ludwig, On Melting of Electrodes during Electro-Slag Remelting, *ISIJ International*., **54**, 1621 (2014).
16. A. Kharicha, M. Wu, A. Ludwig, and E. Karimi-Sibaki, Simulation of the Electric Signal During the Formation and Departure of Droplets in the Electroslag Remelting Process, *Metall. Mater. Trans. B*, **47B**, 1427 (2016).
17. H. Versteeg and W. Malalasekera, An introduction to computational fluid dynamics: the finite method, Pearson Education Limited, Essex, 2007.
18. E. Karimi-Sibaki, A. Kharicha, J. Bohacek, M. Wu, and A. Ludwig, A dynamic mesh-based approach to model melting and shape of an ESR electrode, *Metall. Trans. B*, **46**, 2049 (2015).
19. V. R. Subramanian and R. E. White, Simulating Shape Changes during Electrodeposition Primary and Secondary Current Distribution, *J. Electrochem. Soc.*, **149**(10), C498 (2002).
20. Fluent 16.2 User's Guide, Fluent Inc., 2015.
21. A. Menendez Blanco and J. M. Fernandez Oro, Unsteady numerical simulation of an air-operated piston pump for lubricating greases using dynamic meshes, *Comput. Fluids*, **57**, 138 (2012).
22. E. Karimi-Sibaki, A. Kharicha, M. Wu, A. Ludwig, and J. Bohacek, Toward Modeling of Electrochemical Reactions during Electroslag Remelting (ESR) Process, *Steel Research Int*., **88**, 1700011 (2017).
23. E. Karimi-Sibaki, A. Kharicha, M. Wu, A. Ludwig, and J. Bohacek, Modeling electrochemical transport of ions in the molten $CaF_2$–FeO slag operating under a DC voltage, *Applied Mathematics and Computation*, **357**, 357 (2019).
24. E. Karimi-Sibaki, A. Kharicha, M. Wu, A. Ludwig, and J. Bohacek, Confrontation of the o approach with the ionic transport approach for modeling the electrical behavior of an electrolyte, *Ionics*, **24**, 2157 (2018).
25. E. Karimi-Sibaki, A. Kharicha, M. Wu, A. Ludwig, and J. Bohacek, Contribution of an Electro-Vortex Flow to Primary, Secondary, and Tertiary Electric Current Distribution in an Electrolyte, *J. Electrochem. Soc.*, **165**(11), E604 (2018).
26. G. Mutschke and A. Bund, On the 3D character of the magnetohydrodynamic effect during metal electrodeposition in cuboid cells, *Electrochemistry Communications*, **10**, 597 (2008).
27. M. Rosales and J. L. Nava, Simulations of Turbulent Flow, Mass Transport, and Tertiary Current Distribution on the Cathode of a Rotating Cylinder Electrode Reactor in Continuous Operation Mode during Silver Deposition, *J. Electrochem. Soc.*, **164**, E3345 (2017).